



## Transverse target spin asymmetries in exclusive $\rho^0$ muoproduction



COMPASS Collaboration

C. Adolph<sup>h</sup>, R. Akhunzyanov<sup>g</sup>, M.G. Alekseev<sup>x</sup>, V.Yu. Alexakhin<sup>g</sup>, Yu. Alexandrov<sup>o,1</sup>, G.D. Alexeev<sup>g</sup>, A. Amoroso<sup>aa,ab</sup>, V. Andrieux<sup>v</sup>, V. Anosov<sup>g</sup>, A. Austregesilo<sup>j,q</sup>, B. Badelek<sup>ae</sup>, F. Balestra<sup>aa,ab</sup>, J. Barth<sup>d</sup>, G. Baum<sup>a</sup>, R. Beck<sup>c</sup>, Y. Bedfer<sup>v</sup>, A. Berlin<sup>b</sup>, J. Bernhard<sup>m</sup>, R. Bertini<sup>aa,ab</sup>, K. Bicker<sup>j,q</sup>, J. Bieling<sup>d</sup>, R. Birsa<sup>x</sup>, J. Bisplinghoff<sup>c</sup>, M. Bodlak<sup>s</sup>, M. Boer<sup>v</sup>, P. Bordalo<sup>l,2</sup>, F. Bradamante<sup>y,j</sup>, C. Braun<sup>h</sup>, A. Bravar<sup>x</sup>, A. Bressan<sup>y,x,\*</sup>, M. Büchele<sup>i</sup>, E. Burtin<sup>v</sup>, L. Capozza<sup>v</sup>, M. Chiosso<sup>aa,ab</sup>, S.U. Chung<sup>q,3</sup>, A. Cicuttin<sup>z,x</sup>, M.L. Crespo<sup>z,x</sup>, Q. Curiel<sup>v</sup>, S. Dalla Torre<sup>x</sup>, S.S. Dasgupta<sup>f</sup>, S. Dasgupta<sup>x</sup>, O.Yu. Denisov<sup>ab</sup>, S.V. Donskov<sup>u</sup>, N. Doshita<sup>ag</sup>, V. Duic<sup>y</sup>, W. Dünneweber<sup>p</sup>, M. Dziewiecki<sup>af</sup>, A. Efremov<sup>g</sup>, C. Elia<sup>y,x</sup>, P.D. Eversheim<sup>c</sup>, W. Eyrich<sup>h</sup>, M. Faessler<sup>p</sup>, A. Ferrero<sup>v</sup>, A. Filin<sup>u</sup>, M. Finger<sup>s</sup>, M. Finger Jr.<sup>s</sup>, H. Fischer<sup>i</sup>, C. Franco<sup>l</sup>, N. du Fresne von Hohenesche<sup>m,j</sup>, J.M. Friedrich<sup>q</sup>, V. Frolov<sup>j</sup>, R. Garfagnini<sup>aa,ab</sup>, F. Gautheron<sup>b</sup>, O.P. Gavrichtchouk<sup>g</sup>, S. Gerassimov<sup>o,q</sup>, R. Geyer<sup>p</sup>, M. Giorgi<sup>y,x</sup>, I. Gnesi<sup>aa,ab</sup>, B. Gobbo<sup>x</sup>, S. Goertz<sup>d</sup>, M. Gorzellik<sup>i</sup>, S. Grabmüller<sup>q</sup>, A. Grasso<sup>aa,ab</sup>, B. Grube<sup>q</sup>, R. Gushterski<sup>g</sup>, A. Guskov<sup>g</sup>, T. Guthörl<sup>i,4</sup>, F. Haas<sup>q</sup>, D. von Harrach<sup>m</sup>, D. Hahne<sup>d</sup>, R. Hashimoto<sup>ag</sup>, F.H. Heinsius<sup>i</sup>, F. Herrmann<sup>i</sup>, C. Heß<sup>b</sup>, F. Hinterberger<sup>c</sup>, Ch. Höppner<sup>q</sup>, N. Horikawa<sup>r,5</sup>, N. d'Hose<sup>v</sup>, S. Huber<sup>q</sup>, S. Ishimoto<sup>ag,6</sup>, A. Ivanov<sup>g</sup>, Yu. Ivanshin<sup>g</sup>, T. Iwata<sup>ag</sup>, R. Jahn<sup>c</sup>, V. Jary<sup>t</sup>, P. Jasinski<sup>m</sup>, P. Joerg<sup>i</sup>, R. Joosten<sup>c</sup>, E. Kabuß<sup>m</sup>, D. Kang<sup>m</sup>, B. Ketzer<sup>q</sup>, G.V. Khaustov<sup>u</sup>, Yu.A. Khokhlov<sup>u,7</sup>, Yu. Kisselev<sup>g</sup>, F. Klein<sup>d</sup>, K. Klimaszewski<sup>ad</sup>, J.H. Koivuniemi<sup>b</sup>, V.N. Kolosov<sup>u</sup>, K. Kondo<sup>ag</sup>, K. Königsmann<sup>i</sup>, I. Konorov<sup>o,q</sup>, V.F. Konstantinov<sup>u</sup>, A.M. Kotzinian<sup>aa,ab</sup>, O. Kouznetsov<sup>g</sup>, Z. Kral<sup>t</sup>, M. Krämer<sup>q</sup>, Z.V. Kroumchtein<sup>g</sup>, N. Kuchinski<sup>g</sup>, F. Kunne<sup>v,\*</sup>, K. Kurek<sup>ad</sup>, R.P. Kurjata<sup>af</sup>, A.A. Lednev<sup>u</sup>, A. Lehmann<sup>h</sup>, S. Levorato<sup>x</sup>, J. Lichtenstadt<sup>w</sup>, A. Maggiora<sup>ab</sup>, A. Magnon<sup>v</sup>, N. Makke<sup>y,x</sup>, G.K. Mallot<sup>j</sup>, C. Marchand<sup>v</sup>, A. Martin<sup>y,x</sup>, J. Marzec<sup>af</sup>, J. Matousek<sup>s</sup>, H. Matsuda<sup>ag</sup>, T. Matsuda<sup>n</sup>, G. Meshcheryakov<sup>g</sup>, W. Meyer<sup>b</sup>, T. Michigami<sup>ag</sup>, Yu.V. Mikhailov<sup>u</sup>, Y. Miyachi<sup>ag</sup>, A. Nagaytsev<sup>g</sup>, T. Nagel<sup>q</sup>, F. Nerling<sup>i</sup>, S. Neubert<sup>q</sup>, D. Neyret<sup>v</sup>, V.I. Nikolaenko<sup>u</sup>, J. Novy<sup>t</sup>, W.-D. Nowak<sup>i</sup>, A.S. Nunes<sup>l</sup>, I. Orlov<sup>g</sup>, A.G. Olshevsky<sup>g</sup>, M. Ostrick<sup>m</sup>, R. Panknin<sup>d</sup>, D. Panzieri<sup>ac,ab</sup>, B. Parsamyan<sup>aa,ab</sup>, S. Paul<sup>q</sup>, M. Pesek<sup>s</sup>, D. Peshekhonov<sup>g</sup>, G. Piragino<sup>aa,ab</sup>, S. Platchkov<sup>v</sup>, J. Pochodzalla<sup>m</sup>, J. Polak<sup>k,x</sup>, V.A. Polyakov<sup>u</sup>, J. Pretz<sup>d,8</sup>, M. Quaresma<sup>l</sup>, C. Quintans<sup>l</sup>, S. Ramos<sup>l,2</sup>, G. Reicherz<sup>b</sup>, E. Rocco<sup>j</sup>, V. Rodionov<sup>g</sup>, E. Rondio<sup>ad</sup>, N.S. Rossiyskaya<sup>g</sup>, D.I. Ryabchikov<sup>u</sup>, V.D. Samoylenko<sup>u</sup>, A. Sandacz<sup>ad</sup>, M.G. Sapozhnikov<sup>g</sup>, S. Sarkar<sup>f</sup>, I.A. Savin<sup>g</sup>, G. Sbrizzai<sup>y,x</sup>, P. Schiavon<sup>y,x</sup>, C. Schill<sup>i</sup>, T. Schlüter<sup>p</sup>, A. Schmidt<sup>h</sup>, K. Schmidt<sup>i,4,\*</sup>, L. Schmitt<sup>q,9</sup>, H. Schmüden<sup>c</sup>, K. Schönning<sup>j</sup>, S. Schopferer<sup>i</sup>, M. Schott<sup>j</sup>, O.Yu. Shevchenko<sup>g</sup>, L. Silva<sup>l</sup>, L. Sinha<sup>f</sup>, S. Sirtli<sup>i</sup>, M. Slunecka<sup>g</sup>, S. Sosio<sup>aa,ab</sup>, F. Sozzi<sup>x</sup>, A. Srnka<sup>e</sup>, L. Steiger<sup>x</sup>, M. Stolarski<sup>l</sup>, M. Sulc<sup>k</sup>, R. Sulej<sup>ad</sup>, H. Suzuki<sup>ag,5</sup>, A. Szabelski<sup>ad</sup>, T. Szameitat<sup>i</sup>, P. Sznajder<sup>ad</sup>, S. Takekawa<sup>ab</sup>, J. Ter Wolbeek<sup>i,4</sup>, S. Tessaro<sup>x</sup>, F. Tassarotto<sup>x</sup>,

\* Corresponding authors.

E-mail addresses: [Andrea.Bressan@cern.ch](mailto:Andrea.Bressan@cern.ch) (A. Bressan), [Fabienne.Kunne@cern.ch](mailto:Fabienne.Kunne@cern.ch) (F. Kunne), [Katharina.Schmidt@cern.ch](mailto:Katharina.Schmidt@cern.ch) (K. Schmidt).

F. Thibaud<sup>v</sup>, S. Uhl<sup>q</sup>, I. Uman<sup>p</sup>, M. Vandenbroucke<sup>v</sup>, M. Virius<sup>t</sup>, J. Vondra<sup>t</sup>, L. Wang<sup>b</sup>,  
T. Weisrock<sup>m</sup>, M. Wilfert<sup>m</sup>, R. Windmolders<sup>d</sup>, W. Wiślicki<sup>ad</sup>, H. Wollny<sup>v</sup>, K. Zaremba<sup>af</sup>,  
M. Zavertyaev<sup>o</sup>, E. Zemlyanichkina<sup>g</sup>, N. Zhuravlev<sup>g</sup>, M. Ziembicki<sup>af</sup>

- <sup>a</sup> Universität Bielefeld Fakultät für Physik, 33501 Bielefeld, Germany<sup>10</sup>  
<sup>b</sup> Universität Bochum, Institut für Experimentalphysik, 44780 Bochum, Germany<sup>10,17</sup>  
<sup>c</sup> Universität Bonn, Helmholtz-Institut für Strahlen- und Kernphysik, 53115 Bonn, Germany<sup>10</sup>  
<sup>d</sup> Universität Bonn, Physikalisches Institut, 53115 Bonn, Germany<sup>10</sup>  
<sup>e</sup> Institute of Scientific Instruments, AS CR, 61264 Brno, Czech Republic<sup>11</sup>  
<sup>f</sup> Matrivani Institute of Experimental Research & Education, Calcutta-700 030, India<sup>12</sup>  
<sup>g</sup> Joint Institute for Nuclear Research, 141980 Dubna, Moscow Region, Russia<sup>13</sup>  
<sup>h</sup> Universität Erlangen–Nürnberg, Physikalisches Institut, 91054 Erlangen, Germany<sup>10</sup>  
<sup>i</sup> Universität Freiburg, Physikalisches Institut, 79104 Freiburg, Germany<sup>10,17</sup>  
<sup>j</sup> CERN, 1211 Geneva 23, Switzerland  
<sup>k</sup> Technical University in Liberec, 46117 Liberec, Czech Republic<sup>11</sup>  
<sup>l</sup> LIP, 1000-149 Lisbon, Portugal<sup>14</sup>  
<sup>m</sup> Universität Mainz, Institut für Kernphysik, 55099 Mainz, Germany<sup>10</sup>  
<sup>n</sup> University of Miyazaki, Miyazaki 889-2192, Japan<sup>15</sup>  
<sup>o</sup> Lebedev Physical Institute, 119991 Moscow, Russia  
<sup>p</sup> Ludwig-Maximilians-Universität München, Department für Physik, 80799 Munich, Germany<sup>10,16</sup>  
<sup>q</sup> Technische Universität München, Physik Department, 85748 Garching, Germany<sup>10,16</sup>  
<sup>r</sup> Nagoya University, 464 Nagoya, Japan<sup>15</sup>  
<sup>s</sup> Charles University in Prague, Faculty of Mathematics and Physics, 18000 Prague, Czech Republic<sup>11</sup>  
<sup>t</sup> Czech Technical University in Prague, 16636 Prague, Czech Republic<sup>11</sup>  
<sup>u</sup> State Research Center of the Russian Federation, Institute for High Energy Physics, 142281 Protvino, Russia  
<sup>v</sup> CEA IRFU/SPHN Saclay, 91191 Gif-sur-Yvette, France<sup>17</sup>  
<sup>w</sup> Tel Aviv University, School of Physics and Astronomy, 69978 Tel Aviv, Israel<sup>18</sup>  
<sup>x</sup> Trieste Section of INFN, 34127 Trieste, Italy  
<sup>y</sup> University of Trieste, Department of Physics, 34127 Trieste, Italy  
<sup>z</sup> Abdus Salam ICTP, 34151 Trieste, Italy  
<sup>aa</sup> University of Turin, Department of Physics, 10125 Turin, Italy  
<sup>ab</sup> Torino Section of INFN, 10125 Turin, Italy  
<sup>ac</sup> University of Eastern Piedmont, 15100 Alessandria, Italy  
<sup>ad</sup> National Centre for Nuclear Research, 00-681 Warsaw, Poland<sup>19</sup>  
<sup>ae</sup> University of Warsaw, Faculty of Physics, 00-681 Warsaw, Poland<sup>19</sup>  
<sup>af</sup> Warsaw University of Technology, Institute of Radioelectronics, 00-665 Warsaw, Poland<sup>19</sup>  
<sup>ag</sup> Yamagata University, Yamagata, 992-8510, Japan<sup>15</sup>

## ARTICLE INFO

### Article history:

Received 4 October 2013  
 Received in revised form 30 January 2014  
 Accepted 4 February 2014  
 Available online 14 February 2014  
 Editor: M. Doser

## ABSTRACT

Exclusive production of  $\rho^0$  mesons was studied at the COMPASS experiment by scattering 160 GeV/c muons off transversely polarised protons. Five single-spin and three double-spin azimuthal asymmetries were measured as a function of  $Q^2$ ,  $x_{Bj}$ , or  $p_T^2$ . The  $\sin\phi_S$  asymmetry is found to be  $-0.019 \pm 0.008(\text{stat.}) \pm 0.003(\text{sys.})$ . All other asymmetries are also found to be of small magnitude and consistent with zero within experimental uncertainties. Very recent calculations using a GPD-based model agree well with the present results. The data is interpreted as evidence for the existence of chiral-odd, transverse generalized parton distributions.

© 2014 Elsevier B.V. This is an open access article under the CC BY license (<http://creativecommons.org/licenses/by/3.0/>). Funded by SCOAP<sup>3</sup>.

<sup>1</sup> Deceased.

<sup>2</sup> Also at IST, Universidade Técnica de Lisboa, Lisbon, Portugal.

<sup>3</sup> Also at Department of Physics, Pusan National University, Busan 609-735, Republic of Korea and at Physics Department, Brookhaven National Laboratory, Upton, NY 11973, USA.

<sup>4</sup> Supported by the DFG Research Training Group Programme 1102 “Physics at Hadron Accelerators”.

<sup>5</sup> Also at Chubu University, Kasugai, Aichi, 487-8501, Japan.

<sup>6</sup> Also at KEK, 1-1 Oho, Tsukuba, Ibaraki, 305-0801, Japan.

<sup>7</sup> Also at Moscow Institute of Physics and Technology, Moscow Region, 141700, Russia.

<sup>8</sup> Present address: RWTH Aachen University, III. Physikalisches Institut, 52056 Aachen, Germany.

<sup>9</sup> Also at GSI mbH, Planckstr. 1, D-64291 Darmstadt, Germany.

<sup>10</sup> Supported by the German Bundesministerium für Bildung und Forschung.

<sup>11</sup> Supported by Czech Republic MEYS Grants ME492 and LA242.

<sup>12</sup> Supported by SAIL (CSR), Govt. of India.

<sup>13</sup> Supported by CERN-RFBR Grants 08-02-91009 and 12-02-91500.

<sup>14</sup> Supported by the Portuguese FCT – Fundação para a Ciência e Tecnologia, COMPETE and QREN, Grants CERN/FP/109323/2009, CERN/FP/116376/2010 and CERN/FP/123600/2011.

<sup>15</sup> Supported by the MEXT and the JSPS under the Grants Nos. 18002006, 20540299 and 18540281; Daiko Foundation and Yamada Foundation.

<sup>16</sup> Supported by the DFG cluster of excellence ‘Origin and Structure of the Universe’ ([www.universe-cluster.de](http://www.universe-cluster.de)).

<sup>17</sup> Supported by EU FP7 (HadronPhysics3, Grant Agreement number 283286).

<sup>18</sup> Supported by the Israel Science Foundation, founded by the Israel Academy of Sciences and Humanities.

<sup>19</sup> Supported by the Polish NCN Grant DEC-2011/01/M/ST2/02350.

## 1. Introduction

The spin structure of the nucleon is a key issue in experimental and theoretical research since a few decades. The most general information on the partonic structure of hadrons is contained in the generalised parton correlation functions (GPCFs) [1,2], which parameterise the fully unintegrated, off-diagonal parton-parton correlators for a given hadron. These GPCFs are ‘mother distributions’ of the generalised parton distributions (GPDs) and the transverse momentum dependent parton distributions (TMDs), which can be considered as different projections or limiting cases of GPCFs. While GPDs appear in the QCD-description of hard exclusive processes such as deeply virtual Compton scattering (DVCS) and hard exclusive meson production (HEMP), TMDs can be measured in reactions like semi-inclusive deep inelastic scattering (SIDIS) or Drell–Yan processes. The GPDs and TMDs provide complementary 3-dimensional pictures of the nucleon. In particular, when Fourier-transformed to impact parameter space and for the case of vanishing longitudinal momentum transfer, GPDs provide a three dimensional description of the nucleon in a mixed momentum-coordinate space, also known as ‘nucleon tomography’ [3,4]. Moreover, GPDs and TMDs contain information on the orbital motion of partons inside the nucleon.

The process amplitude for hard exclusive meson production by *longitudinal* virtual photons was proven rigorously to factorise into a hard-scattering part and a soft part [5,6]. The hard part is calculable in perturbative QCD (pQCD). The soft part contains GPDs to describe the structure of the probed nucleon and a distribution amplitude (DA) to describe the one of the produced meson. This collinear factorisation holds in the generalised Bjorken limit of large photon virtuality  $Q^2$  and large total energy in the virtual-photon nucleon system,  $W$ , but fixed  $x_{Bj}$ , and for  $|t|/Q^2 \ll 1$ . Here  $t$  is the four-momentum transfer to the proton and  $x_{Bj} = Q^2/2M_p\nu$ , where  $\nu$  is the energy of the virtual photon in the lab frame and  $M_p$  the proton mass.

For hard exclusive meson production by *transverse* virtual photons, no proof of collinear factorisation exists. In phenomenological pQCD-inspired models  $k_\perp$  factorisation is used, where  $k_\perp$  denotes the parton transverse momentum. In the model of Refs. [7–9], electroproduction of a light vector meson  $V$  at small  $x_{Bj}$  is analysed in the ‘handbag’ approach, in which the amplitude of the process is a convolution of GPDs with amplitudes for the partonic subprocesses  $\gamma^*q \rightarrow Vq$  and  $\gamma^*g \rightarrow Vg$ . Here,  $q$  and  $g$  denote quarks and gluons, respectively. The partonic subprocess amplitudes, which comprise corresponding hard scattering kernels and meson DAs, are calculated in the modified perturbative approach where the transverse momenta of quark and antiquark forming the vector meson are retained and Sudakov suppressions are taken into account. The partons are still emitted and reabsorbed from the nucleon collinear to the nucleon momentum. In such models, cross sections and also spin-density matrix elements for HEMP by both longitudinal and transverse virtual photons can be well described simultaneously [7,10].

At leading twist, the chiral-even GPDs  $H^f$  and  $E^f$ , where  $f$  denotes a quark of a given flavor or a gluon, are sufficient to describe exclusive vector meson production on a spin 1/2 target. These GPDs are of special interest as they are related to the total angular momentum carried by partons in the nucleon [11]. A variety of GPD fits using all existing DVCS proton data has shown that the GPDs  $H^f$  are well constrained over the presently limited accessible  $x_{Bj}$  range, by the very low  $x_{Bj}$  data of the HERA collider and by the high  $x_{Bj}$  data of HERMES and JLab [12–15]. There exist constraints on GPDs  $E^f$  for valence quarks from fits to nucleon form factor data [16], HERMES transverse proton data [17] and JLab neutron data [18]. A parameterisation of chiral-even GPDs [9], which is

consistent with the HEMP data of HERMES [19] and COMPASS [20], was recently demonstrated to successfully describe almost all existing DVCS data [21]. This is clear evidence for the consistency of the contemporary phenomenological GPD-based description of both DVCS and HEMP.

There exist also chiral-odd – often called transverse – GPDs, from which in particular  $H_T^f$  and  $\bar{E}_T^f$  were shown to be required [22,23] for the description of exclusive  $\pi^+$  electroproduction on a transversely polarised proton target [24]. It was recently shown [25] that the data analysed in this Letter are also sensitive to these GPDs.

This Letter describes the measurement of exclusive  $\rho^0$  muoproduction on transversely polarised protons with the COMPASS apparatus. Size and kinematic dependences of azimuthal modulations of the cross section with respect to beam and target polarisation are determined and discussed, in particular in terms of the above introduced chiral-odd GPDs.

## 2. Formalism

The cross section for exclusive  $\rho^0$  muoproduction,  $\mu N \rightarrow \mu' \rho^0 N'$ , on a transversely polarised target reads<sup>20</sup> [26]<sup>21</sup>:

$$\begin{aligned} & \frac{d\sigma}{dx_{Bj} dQ^2 dt d\phi d\phi_S} \\ &= \left[ \frac{\alpha_{em}}{8\pi^3} \frac{y^2}{1-\varepsilon} \frac{1-x_{Bj}}{x_{Bj}} \frac{1}{Q^2} \right] \left\{ \frac{1}{2} (\sigma_{++}^{++} + \sigma_{++}^{--}) + \varepsilon \sigma_{00}^{++} \right. \\ & \quad - \varepsilon \cos(2\phi) \operatorname{Re} \sigma_{+-}^{++} - \sqrt{\varepsilon(1+\varepsilon)} \cos \phi \operatorname{Re} (\sigma_{+0}^{++} + \sigma_{+0}^{--}) \\ & \quad - P_\ell \sqrt{\varepsilon(1-\varepsilon)} \sin \phi \operatorname{Im} (\sigma_{+0}^{++} + \sigma_{+0}^{--}) \\ & \quad - S_T \left[ \sin(\phi - \phi_S) \operatorname{Im} (\sigma_{++}^{+-} + \varepsilon \sigma_{00}^{+-}) \right. \\ & \quad \left. + \frac{\varepsilon}{2} \sin(\phi + \phi_S) \operatorname{Im} \sigma_{+-}^{+-} + \frac{\varepsilon}{2} \sin(3\phi - \phi_S) \operatorname{Im} \sigma_{+-}^{--} \right. \\ & \quad \left. + \sqrt{\varepsilon(1+\varepsilon)} \sin \phi_S \operatorname{Im} \sigma_{+0}^{+-} \right. \\ & \quad \left. + \sqrt{\varepsilon(1+\varepsilon)} \sin(2\phi - \phi_S) \operatorname{Im} \sigma_{+0}^{--} \right] \\ & \quad + S_T P_\ell \left[ \sqrt{1-\varepsilon^2} \cos(\phi - \phi_S) \operatorname{Re} \sigma_{++}^{+-} \right. \\ & \quad - \sqrt{\varepsilon(1-\varepsilon)} \cos \phi_S \operatorname{Re} \sigma_{+0}^{+-} \\ & \quad \left. - \sqrt{\varepsilon(1-\varepsilon)} \cos(2\phi - \phi_S) \operatorname{Re} \sigma_{+0}^{--} \right] \left. \right\}. \quad (1) \end{aligned}$$

Here,  $S_T$  is the target spin component perpendicular to the direction of the virtual photon. The beam polarisation is denoted by  $P_\ell$ . The azimuthal angle between the lepton scattering plane and the production plane spanned by virtual photon and produced meson is denoted by  $\phi$ , whereas  $\phi_S$  is the azimuthal angle of the target spin vector about the virtual-photon direction relative to the lepton scattering plane (see Fig. 1). The  $S_T$  dependent part of Eq. (1) contains eight different azimuthal modulations: five sine modulations for the case of an unpolarised beam and three cosine modulations for the case of a longitudinally polarised beam. Neglecting terms depending on  $m_\mu^2/Q^2$ , where  $m_\mu$  denotes the mass of the incoming lepton, the virtual-photon polarisation parameter  $\varepsilon$  describes the ratio of longitudinal and transverse photon fluxes and is given by:

<sup>20</sup> For convenience in this chapter natural units  $\hbar = c = 1$  are used.

<sup>21</sup> Note that the  $t$ -dependence of the cross section is indicated explicitly here and the definition of  $\sigma_{\mu\sigma}^{\nu\lambda}$  given by Eq. (3) slightly differs from that in Ref. [26].

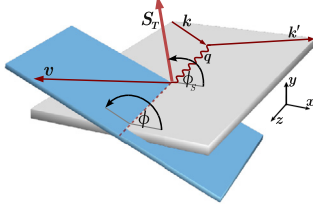


**Fig. 1.** Definition of the angles  $\phi$  and  $\phi_s$ . Here  $\mathbf{k}$ ,  $\mathbf{k}'$ ,  $\mathbf{q}$  and  $\mathbf{v}$  represent three-momentum vectors of the incident and the scattered muon, the virtual photon and the meson respectively. The symbol  $S_T$  denotes the component of the target spin vector perpendicular to the virtual-photon direction.

$$\varepsilon = \frac{1 - y - \frac{1}{4}y^2\gamma^2}{1 - y + \frac{1}{2}y^2 + \frac{1}{4}y^2\gamma^2}, \quad \gamma = \frac{2M_p x_{Bj}}{Q}, \quad (2)$$

where  $y$  is the fractional energy of the virtual photon. The symbols  $\sigma_{\mu\sigma}^{\nu\lambda}$  in Eq. (1) stand for polarised photoabsorption cross sections or interference terms, which are given as products of helicity amplitudes  $\mathcal{M}$ :

$$\sigma_{\mu\sigma}^{\nu\lambda} = \sum \mathcal{M}_{\mu'\nu',\mu\nu}^* \mathcal{M}_{\mu'\nu',\sigma\lambda}, \quad (3)$$

where the sum runs over  $\mu' = 0, \pm 1$  and  $\nu' = \pm 1/2$ . The helicity amplitude labels appear in the following order: vector meson ( $\mu'$ ), final-state proton ( $\nu'$ ), photon ( $\mu$  or  $\sigma$ ), initial-state proton ( $\nu$  or  $\lambda$ ). For brevity, the helicities  $-1, -1/2, 0, 1/2, 1$  will be labelled by only their signs or zero, omitting 1 or  $1/2$ , respectively. Also the dependence of  $\sigma_{\mu\sigma}^{\nu\lambda}$  on kinematic variables is omitted.

The amplitudes of those cross section modulations that depend on target polarisation are obtained from Eq. (1) as follows:

$$\begin{aligned} A_{\text{UT}}^{\sin(\phi-\phi_s)} &= -\frac{\text{Im}(\sigma_{++}^{+-} + \varepsilon\sigma_{00}^{+-})}{\sigma_0}, & A_{\text{LT}}^{\cos(\phi-\phi_s)} &= \frac{\text{Re}\sigma_{++}^{+-}}{\sigma_0}, \\ A_{\text{UT}}^{\sin(\phi+\phi_s)} &= -\frac{\text{Im}\sigma_{+-}^{+-}}{\sigma_0}, & A_{\text{LT}}^{\cos\phi_s} &= -\frac{\text{Re}\sigma_{+0}^{+-}}{\sigma_0}, \\ A_{\text{UT}}^{\sin(3\phi-\phi_s)} &= -\frac{\text{Im}\sigma_{+-}^{+-}}{\sigma_0}, & A_{\text{LT}}^{\cos(2\phi-\phi_s)} &= -\frac{\text{Re}\sigma_{+0}^{+-}}{\sigma_0}, \\ A_{\text{UT}}^{\sin\phi_s} &= -\frac{\text{Im}\sigma_{+0}^{+-}}{\sigma_0}, \\ A_{\text{UT}}^{\sin(2\phi-\phi_s)} &= -\frac{\text{Im}\sigma_{+0}^{+-}}{\sigma_0}. \end{aligned} \quad (4)$$

Here, unpolarised (longitudinally polarised) beam is denoted by U (L) and transverse target polarisation by T. The  $\phi$ -independent part of the cross section for unpolarised beam and target, denoted by  $\sigma_0$ , is given as a sum of the transverse and longitudinal cross sections:

$$\sigma_0 = \frac{1}{2}(\sigma_{++}^{++} + \sigma_{++}^{--}) + \varepsilon\sigma_{00}^{++}. \quad (5)$$

The amplitudes given in Eq. (4) will be referred to as asymmetries in the rest of the Letter.

### 3. Experimental set-up

The COMPASS experiment is situated at the high-intensity M2 muon beam of the CERN SPS. A detailed description can be found in Ref. [27].

The  $\mu^+$  beam had a nominal momentum of 160 GeV/c with a spread of 5% and a longitudinal polarisation of  $P_\ell \approx -0.8$ . The data were taken at a mean intensity of  $3.5 \cdot 10^8 \mu/\text{spill}$ , for a spill length of about 10 s every 40 s. A measurement of the trajectory and the

momentum of each incoming muon is performed upstream of the target.

The beam traverses a solid-state ammonia ( $\text{NH}_3$ ) target that provides transversely polarised protons. The target is situated within a large aperture magnet with a dipole holding field of 0.5 T. The 2.5 T solenoidal field is only used when polarising the target material. A mixture of liquid  $^3\text{He}$  and  $^4\text{He}$  is used to cool the target to 50 mK. Ten NMR coils surrounding the target allow for a determination of the target polarisation  $P_T$ , which typical amounts to 0.8 with an uncertainty of 3%. The ammonia is contained in three cylindrical target cells with a diameter of 4 cm, placed one after another along the beam. The central cell is 60 cm long and the two outer ones are 30 cm long, with 5 cm space between cells. The spin directions in neighbouring cells are opposite. Such a target configuration allows for a simultaneous measurement of azimuthal asymmetries for the two target spin directions in order to become independent of beam flux measurements. Systematic effects due to acceptance are reduced by reversing the spin directions on a weekly basis. With the three-cell configuration, the average acceptance for cells with opposite spin direction is approximately the same, which leads to a further reduction of systematic uncertainties.

The dilution factor  $f$ , which is the cross-section-weighted fraction of polarisable material, is calculated for incoherent exclusive  $\rho^0$  production using the measured material composition and the nuclear dependence of the cross section:

$$f = \frac{n_p}{n_p + \sum_A n_A \frac{\sigma_A}{\sigma_p}}. \quad (6)$$

Here,  $n_p$  and  $n_A$  denote the numbers of polarisable protons in the target and of unpolarised nucleons in the target material with atomic mass  $A$ , respectively. The sum runs over all nuclei present in the COMPASS target. The ratio of this cross section per nucleon for a given nucleus to the cross section on the proton is parameterised according to Eq. (11) in Ref. [28] over a wide range of  $Q^2$ , using measurements on various nuclear targets as described therein. No dependence of nuclear effects on  $\nu$  and on  $p_T^2$  is assumed as motivated by the NMC results on incoherent exclusive  $\rho^0$  production [29] in a kinematic range similar to that of COMPASS. For the  $\text{NH}_3$  target the dilution factor amounts typically to 0.25 [20].

The spectrometer consists of two stages in order to reconstruct scattered muons and produced hadrons over wide momentum and angular ranges. Each stage has a dipole magnet with tracking detectors before and after the magnet, hadron and electromagnetic calorimeters and muon identification. Identification of charged tracks with a RICH detector in the first stage is not used in the present analysis.

Inclusive and calorimetric triggers are used to activate data recording. Inclusive triggers select scattered muons using pairs of hodoscopes and muon absorbers. They are complemented by a calorimetric trigger that relies on the energy deposit of hadrons in one of the calorimeters. This trigger covers small acceptance holes in the inclusive triggers. It was checked that this trigger does not introduce any bias due to the acceptance of the calorimeters in the  $x_{Bj}$  range covered by the present data [30]. Veto counters upstream of the target are used to suppress beam halo muons.

### 4. Event selection and background estimation

The presented work is a continuation of the analysis of  $A_{\text{UT}}^{\sin(\phi-\phi_s)}$  for exclusive  $\rho^0$  mesons produced off transversely polarised protons at COMPASS and it is based on the same proton event sample as in Ref. [20]. The essential steps of event selection and asymmetry extraction are summarised in the following.

The considered events are characterised by an incoming and a scattered muon and two oppositely charged hadrons,  $h^+h^-$ , with all four tracks associated to a common vertex in the polarised target. In order to select events in the deep inelastic scattering regime and suppress radiative corrections, the following cuts are used:  $Q^2 > 1$  (GeV/c)<sup>2</sup>,  $0.003 < x_{Bj} < 0.35$ ,  $W > 5$  GeV/c<sup>2</sup> and  $0.1 < y < 0.9$ . The production of  $\rho^0$  mesons is selected in the two-hadron invariant mass range  $0.5 \text{ GeV}/c^2 < M_{\pi^+\pi^-} < 1.1 \text{ GeV}/c^2$ , where for each hadron the pion mass hypothesis is assigned. This cut is optimised towards high yield and purity of  $\rho^0$  production, as compared to non-resonant  $\pi^+\pi^-$  production. The measurements are performed without detection of the recoiling proton in the final state. Exclusive events are selected by choosing a range in missing energy,

$$E_{\text{miss}} = \frac{(p + q - v)^2 - p^2}{2M_p} = v - E_{\rho^0} + \frac{t}{2M_p}. \quad (7)$$

The four-momenta of proton, photon, and meson, are denoted by  $p$ ,  $q$ , and  $v$  respectively. Although for exclusive events  $E_{\text{miss}} \approx 0$  holds, the finite experimental resolution is taken into account by selecting events in the range  $|E_{\text{miss}}| < 2.5$  GeV, which corresponds to  $0 \pm 2\sigma$  where  $\sigma$  is the width of the Gaussian signal peak. Non-exclusive background can be suppressed by cuts on the squared transverse momentum of the vector meson with respect to the virtual-photon direction,  $p_T^2 < 0.5$  (GeV/c)<sup>2</sup>, the energy of the  $\rho^0$  in the laboratory system,  $E_{\rho^0} > 15$  GeV, and the photon virtuality,  $Q^2 < 10$  (GeV/c)<sup>2</sup>. An additional cut  $p_T^2 > 0.05$  (GeV/c)<sup>2</sup> is used to reduce coherently produced events. As explained in Ref. [20] we use  $p_T^2$  rather than  $t$ . After the application of all cuts, the final data set of incoherently produced exclusive  $\rho^0$  events consist of about 797 000 events. The average values of the kinematic variables are  $\langle Q^2 \rangle = 2.15$  (GeV/c)<sup>2</sup>,  $\langle x_{Bj} \rangle = 0.039$ ,  $\langle y \rangle = 0.24$ ,  $\langle W \rangle = 8.13$  GeV/c<sup>2</sup>, and  $\langle p_T^2 \rangle = 0.18$  (GeV/c)<sup>2</sup>. In order to correct for the remaining semi-inclusive background in the signal region, the  $E_{\text{miss}}$  shape of the background is parameterised for each individual target cell in every kinematic bin of  $Q^2$ ,  $x_{Bj}$ , or  $p_T^2$  using a LEPTO Monte Carlo (MC) sample generated with COMPASS tuning [31] of the JETSET parameters. The  $h^+h^-$  MC event sample is weighted in every  $E_{\text{miss}}$  bin  $i$  by the ratio of numbers of  $h^\pm h^\pm$  events from data and MC,

$$w_i = \frac{N_{i,\text{data}}^{h^+h^+}(E_{\text{miss}}) + N_{i,\text{data}}^{h^-h^-}(E_{\text{miss}})}{N_{i,\text{MC}}^{h^+h^+}(E_{\text{miss}}) + N_{i,\text{MC}}^{h^-h^-}(E_{\text{miss}})}, \quad (8)$$

which improves the agreement between data and MC significantly [20].

For each kinematic bin, target cell, and spin orientation a signal plus background fit is performed, whereby a Gaussian function is used for the signal shape, and the background shape is fixed by MC as described above. The fraction of semi-inclusive background in the signal range is 22%, nevertheless the fraction strongly depends on kinematics and varies between 7% and 40%. An example is presented in Fig. 2. The background corrected distributions,  $N_k^{\text{sig}}(\phi, \phi_S)$ , are obtained from the measured distributions in the signal region,  $N_k^{\text{sig,raw}}(\phi, \phi_S)$ , and in the background region  $7 \text{ GeV} < E_{\text{miss}} < 20 \text{ GeV}$ ,  $N_k^{\text{back}}(\phi, \phi_S)$ . The distributions  $N_k^{\text{back}}(\phi, \phi_S)$  are rescaled with the estimated numbers of background events in the signal region and afterwards subtracted from the  $N_k^{\text{sig,raw}}(\phi, \phi_S)$  distributions. As no kinematic dependence of the semi-inclusive background asymmetries, which were small, was observed in the background region, no systematic uncertainty is assigned due to extrapolation of this background into the  $E_{\text{miss}}$  region of the signal.

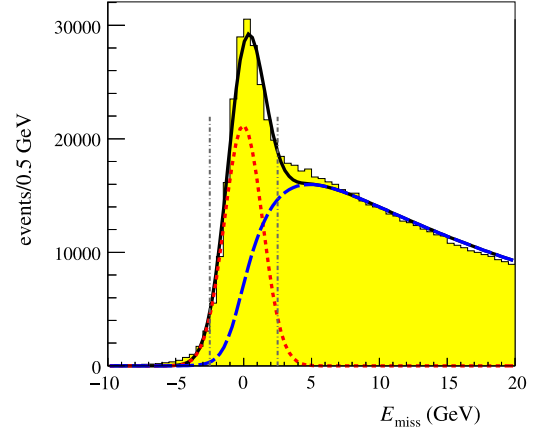


**Fig. 2.** The  $E_{\text{miss}}$  distribution in the range  $2.4 \text{ (GeV}/c)^2 < Q^2 \leq 10 \text{ (GeV}/c)^2$ , together with the signal plus background fits (solid curve). The dotted and dashed curves represent the signal and background contributions, respectively. In the signal region  $-2.5 \text{ GeV} < E_{\text{miss}} < 2.5 \text{ GeV}$ , indicated by vertical dash-dotted lines, the amount of semi-inclusive background is 35%. Averaged over the kinematic bins, the fraction of semi-inclusive background in the signal region is 22%.

After the described subtraction of semi-inclusive background, the final sample still contains diffractive events where the recoiling nucleon is in an excited  $N^*$  or  $\Delta$  state (14%), coherently produced  $\rho^0$  mesons ( $\sim 12\%$ ), and non-resonant  $\pi^+\pi^-$  pairs ( $< 2\%$ ) [20]. We do not apply corrections for these contributions.

## 5. Results and discussion

The asymmetries are evaluated using the background-corrected distributions  $N_k^{\text{sig}}(\phi, \phi_S)$  by combining data-taking periods with opposite target polarisations which are denoted by  $\pm$ . The events of the two outer target cells are summed up. The number of exclusive  $\rho^0$  mesons as a function of  $\phi$  and  $\phi_S$ , where the index  $j$  denotes the  $(\phi, \phi_S)$  bin, can be written for every target cell  $n$  as:

$$N_{j,n}^\pm(\phi, \phi_S) = a_{j,n}^\pm (1 \pm A(\phi, \phi_S)). \quad (9)$$

Here,  $a_{j,n}^\pm$  is the product of spin-averaged cross section, muon flux, number of target nucleons, acceptance, and efficiency of the spectrometer. The angular dependence reads:

$$\begin{aligned} A(\phi, \phi_S) = & A_{\text{UT,raw}}^{\sin(\phi-\phi_S)} \sin(\phi - \phi_S) + A_{\text{UT,raw}}^{\sin(\phi+\phi_S)} \sin(\phi + \phi_S) \\ & + A_{\text{UT,raw}}^{\sin(3\phi-\phi_S)} \sin(3\phi - \phi_S) \\ & + A_{\text{UT,raw}}^{\sin(2\phi-\phi_S)} \sin(2\phi - \phi_S) \\ & + A_{\text{LT,raw}}^{\sin \phi_S} \sin \phi_S + A_{\text{LT,raw}}^{\cos(\phi-\phi_S)} \cos(\phi - \phi_S) \\ & + A_{\text{LT,raw}}^{\cos \phi_S} \cos \phi_S + A_{\text{LT,raw}}^{\cos(2\phi-\phi_S)} \cos(2\phi - \phi_S). \end{aligned} \quad (10)$$

The symbol  $A_{\text{UT(LT),raw}}^m$  denotes the amplitude for the angular modulation  $m$ . After the subtraction of semi-inclusive background, the “raw” asymmetries  $A_{\text{UT,raw}}^m$  and  $A_{\text{LT,raw}}^m$  are extracted from the final sample using a two-dimensional binned maximum likelihood fit with 12 bins in  $\phi$  and in  $\phi_S$ . They are used to obtain the transverse target asymmetries  $A_{\text{UT(LT)}}^m$  defined in Eq. (4) as:

$$\begin{aligned} A_{\text{UT}}^m &= \frac{A_{\text{UT,raw}}^m}{\langle f \cdot |P_T| \cdot D^m(\epsilon) \rangle}, \\ A_{\text{LT}}^m &= \frac{A_{\text{LT,raw}}^m}{\langle f \cdot |P_T| \cdot P_\ell \cdot D^m(\epsilon) \rangle}, \end{aligned} \quad (11)$$

**Table 1**

Systematic uncertainties for the average asymmetries obtained from the studies explained in the text.

|                               | i)    | ii)   | iii)  |
|-------------------------------|-------|-------|-------|
| $A_{UT}^{\sin(\phi-\phi_S)}$  | 0.002 | 0.002 | 0.001 |
| $A_{UT}^{\sin(\phi+\phi_S)}$  | 0.004 | 0.004 | 0.004 |
| $A_{UT}^{\sin(2\phi-\phi_S)}$ | 0.002 | 0.001 | 0.002 |
| $A_{UT}^{\sin(3\phi-\phi_S)}$ | 0.006 | 0.003 | 0.003 |
| $A_{UT}^{\sin\phi_S}$         | 0.001 | 0.003 | 0.001 |
| $A_{LT}^{\cos(\phi-\phi_S)}$  | 0.005 | 0.011 | 0.023 |
| $A_{LT}^{\cos(2\phi-\phi_S)}$ | 0.016 | 0.016 | 0.018 |
| $A_{LT}^{\cos\phi_S}$         | 0.006 | 0.029 | 0.023 |

in every kinematic bin. The denominator is computed using the arithmetic mean of the product that is calculated for each individual event. Here,  $P_T$  is used, which in COMPASS kinematics is a good approximation to  $S_T$ . The depolarisation factors are given by:

$$\begin{aligned}
 D^{\sin(\phi-\phi_S)} &= 1, \\
 D^{\sin(\phi+\phi_S)} &= D^{\sin(3\phi-\phi_S)} = \frac{\varepsilon}{2}, \\
 D^{\sin\phi_S} &= D^{\sin(2\phi-\phi_S)} = \sqrt{\varepsilon(1+\varepsilon)}, \\
 D^{\cos(\phi-\phi_S)} &= \sqrt{1-\varepsilon^2}, \\
 D^{\cos\phi_S} &= D^{\cos(2\phi-\phi_S)} = \sqrt{\varepsilon(1-\varepsilon)}.
 \end{aligned} \tag{12}$$

In order to estimate the systematic uncertainty of the measurements, we take into account the relative uncertainty of the target dilution factor (2%), the target polarisation (3%), and the beam polarisation (5%). Combined in quadrature this gives an overall systematic normalisation uncertainty of 3.6% for the asymmetries  $A_{UT}^m$  and 6.2% for  $A_{LT}^m$ . Additional systematic uncertainties are obtained from separate studies of i) a possible bias of the applied estimator, ii) the stability of the asymmetries over data-taking time, and iii) the robustness of the applied background subtraction method and a difference between the mean asymmetries obtained in the  $x_{Bj}$ ,  $Q^2$  and  $p_T^2$  binning, which is originating from averaging the depolarisation factors. A summary of these three systematic uncertainties for the average asymmetries can be found in Table 1. The total systematic uncertainty is obtained as a quadratic sum of these three components and the normalisation uncertainty.

In Eq. (1),  $S_T$  is defined with respect to the virtual-photon momentum direction, while in the experiment transverse polarisation  $P_T$  is defined relative to the beam direction. The transition from  $S_T$  to  $P_T$  introduces in the cross section [26] the angle  $\theta$  between the virtual photon and the beam direction, which is small at COMPASS kinematics. Additionally, some of the  $A_{UT(LT)}$  asymmetries get mixed with  $A_{UL(LL)}$  asymmetries that are suppressed by  $\sin\theta$ . Presently the influence of the  $\theta$ -related corrections can only be studied based on a few available measurements [32,33] of the double-spin asymmetry  $A_{LL}$  for proton targets in the kinematic range similar to that of COMPASS. Taking into account the smallness of  $\sin\theta$  at COMPASS ( $\sin\theta \approx 0.04$  on average), the correction was found to be negligible. We provide the values of  $\sin\theta$  in the Durham data base [34] to allow for corrections when new or more precise data on  $A_{UL(LL)}$  become available.

The results for the five single-spin and three double-spin asymmetries as a function of  $x_{Bj}$ ,  $Q^2$ , or  $p_T^2$  are shown in Figs. 3 and 4, respectively. Error bars show statistical uncertainties. The systematic uncertainties including the normalisation uncertainties added in quadrature are represented by grey shaded bands. Average asymmetry values for all modulations are given in Fig. 5 and Table 2. For three of them, the experimental precision is as high as  $\mathcal{O}(\pm 0.01)$ . All average asymmetry values are found to

**Table 2**

Average asymmetries with statistical and systematic uncertainties for all measured modulations.

|                               |                              |
|-------------------------------|------------------------------|
| $A_{UT}^{\sin(\phi-\phi_S)}$  | $-0.008 \pm 0.011 \pm 0.003$ |
| $A_{UT}^{\sin(\phi+\phi_S)}$  | $-0.028 \pm 0.022 \pm 0.006$ |
| $A_{UT}^{\sin(2\phi-\phi_S)}$ | $0.004 \pm 0.008 \pm 0.003$  |
| $A_{UT}^{\sin(3\phi-\phi_S)}$ | $0.030 \pm 0.024 \pm 0.008$  |
| $A_{UT}^{\sin\phi_S}$         | $-0.019 \pm 0.008 \pm 0.003$ |
| $A_{LT}^{\cos(\phi-\phi_S)}$  | $0.065 \pm 0.047 \pm 0.026$  |
| $A_{LT}^{\cos(2\phi-\phi_S)}$ | $0.067 \pm 0.071 \pm 0.029$  |
| $A_{LT}^{\cos\phi_S}$         | $-0.094 \pm 0.065 \pm 0.038$ |

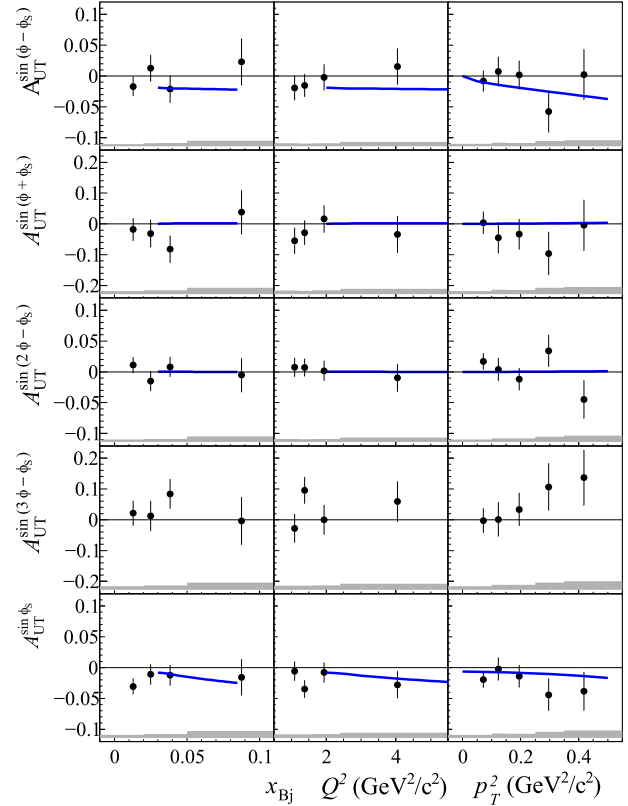


**Fig. 3.** Single-spin azimuthal asymmetries for a transversely (T) polarised target and unpolarised (U) beam. The error bars (bands) represent the statistical (systematic) uncertainties. The curves show the predictions of the GPD model [25]. They are calculated for the average  $W$ ,  $Q^2$  and  $p_T^2$  of our data set,  $W = 8.1$  GeV/ $c^2$  and  $p_T^2 = 0.2$  (GeV/ $c^2$ )<sup>2</sup> for the left and middle panels, and at  $W = 8.1$  GeV/ $c^2$  and  $Q^2 = 2.2$  (GeV/ $c^2$ )<sup>2</sup> for the right panels. The asymmetry  $A_{UT}^{\sin(3\phi-\phi_S)}$  is assumed to be zero in this model.

be of small magnitude, below 0.1. Except  $A_{UT}^{\sin\phi_S}$ , all other average asymmetry values are consistent with zero within experimental uncertainties. All results, including the numerical values for the correlations between the asymmetries, are available in the Durham data base [34]. The five single-spin and three double-spin asymmetries are extracted simultaneously. The result includes a refined evaluation of the earlier published asymmetry  $A_{UT}^{\sin(\phi-\phi_S)}$  [20]. Although both analyses use the same data, the change of the analysis method results in different statistical fluctuations, which implies that the final data samples used here and in [20] are not fully correlated.

As already mentioned above, there exists presently only the model of Refs. [7–9] to describe hard exclusive  $\rho^0$  leptonproduction using GPDs. It is a phenomenological ‘handbag’ approach based on  $k_\perp$  factorisation, which also includes twist-3 meson wave

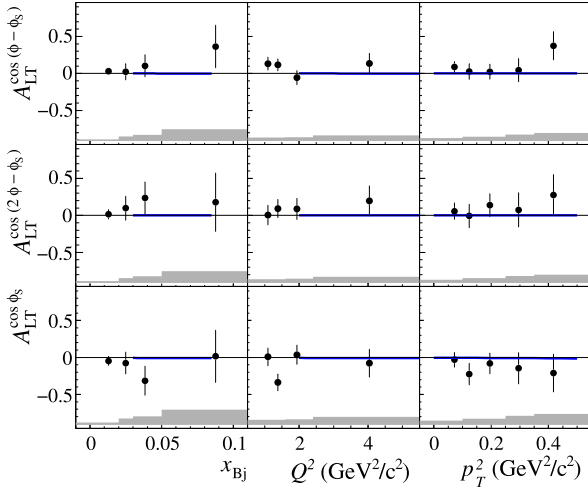


**Fig. 4.** Double-spin azimuthal asymmetries for a transversely (T) polarised target and a longitudinally (L) polarised beam. The error bars (bands) represent the statistical (systematic) uncertainties. They are calculated for the average  $W$ ,  $Q^2$  and  $p_T^2$  of our data set,  $W = 8.1 \text{ GeV}/c^2$  and  $p_T^2 = 0.2 \text{ (GeV}/c)^2$  for the left and middle panels, and at  $W = 8.1 \text{ GeV}/c^2$  and  $Q^2 = 2.2 \text{ (GeV}/c)^2$  for the right panels.

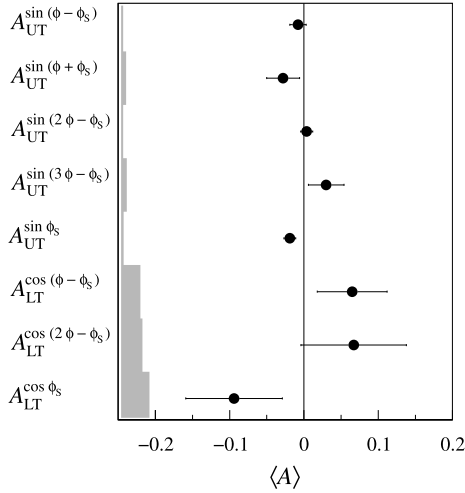


**Fig. 5.** Mean value  $\langle A \rangle$  and the statistical error for every modulation. The error bars (left bands) represent the statistical (systematic) uncertainties.

functions. Calculations for the full set of five  $A_{UT}$  and three  $A_{LT}$  asymmetries were performed very recently [25]. They are shown in Figs. 3, 4 as curves together with the data points. Of particular interest is the level of agreement between data and model calculations for the following four asymmetries, as they involve chiral-odd GPDs [25]:

$$A_{UT}^{\sin(\phi - \phi_s)} \sigma_0 = -2 \text{Im} \left[ \epsilon \mathcal{M}_{0-,0+}^* \mathcal{M}_{0+,0+} + \mathcal{M}_{+-,++}^* \mathcal{M}_{+,++} + \frac{1}{2} \mathcal{M}_{0-,++}^* \mathcal{M}_{0+,++} \right], \quad (13)$$

$$A_{UT}^{\sin \phi_s} \sigma_0 = -\text{Im} \left[ \mathcal{M}_{0-,++}^* \mathcal{M}_{0+,0+} - \mathcal{M}_{0+,++}^* \mathcal{M}_{0-,0+} \right], \quad (14)$$

$$A_{UT}^{\sin(2\phi - \phi_s)} \sigma_0 = -\text{Im} \left[ \mathcal{M}_{0+,++}^* \mathcal{M}_{0-,0+} \right], \quad (15)$$

$$A_{LT}^{\cos \phi_s} \sigma_0 = -\text{Re} \left[ \mathcal{M}_{0-,++}^* \mathcal{M}_{0+,0+} - \mathcal{M}_{0+,++}^* \mathcal{M}_{0-,0+} \right]. \quad (16)$$

Here, the dominant  $\gamma_L^* \rightarrow \rho_L^0$  transitions are described by helicity amplitudes  $\mathcal{M}_{0+,0+}$  and  $\mathcal{M}_{0-,0+}$ , which are related to chiral-even GPDs  $H$  and  $E$ , respectively. The subscripts  $L$  and  $T$  denote the

photon and meson helicities  $0$  and  $\pm 1$ , respectively. These GPDs are used since several years to describe DVCS and HEMP data. The suppressed  $\gamma_T^* \rightarrow \rho_T^0$  transitions are described by the helicity amplitudes  $\mathcal{M}_{+,+,+}$  and  $\mathcal{M}_{+-,++}$ , which are likewise related to  $H$  and  $E$ . By the recent inclusion of transverse, i.e. chiral-odd GPDs, it became possible to also describe  $\gamma_T^* \rightarrow \rho_L^0$  transitions. In their description appear the amplitudes  $\mathcal{M}_{0-,++}$  related to chiral-odd GPDs  $H_T$  [23,25] and  $\mathcal{M}_{0+,++}$  related to chiral-odd GPDs  $\bar{E}_T$  [22]. The double-flip amplitude  $\mathcal{M}_{0-,+}$  is neglected. The transitions  $\gamma_L^* \rightarrow \rho_T^0$  and  $\gamma_T^* \rightarrow \rho_{-T}^0$  are known to be suppressed and hence neglected in the model calculations.

All measured asymmetries agree well with the calculations of Ref. [25]. In Eq. (13), the first two terms represent each a combination of chiral-even GPDs  $H$  and  $E$ . The inclusion of chiral-odd GPDs by the third term has negligible impact on the behaviour of  $A_{UT}^{\sin(\phi - \phi_s)}$ , as can be seen when comparing calculations of Refs. [9] and [25]. The asymmetry  $A_{UT}^{\sin(\phi - \phi_s)}$  itself may still be of small magnitude, because for GPDs  $E$  in  $\rho^0$  production the valence quark contribution is expected to be not large. This is interpreted as a cancellation due to different signs and comparable magnitudes of GPDs  $E^u$  and  $E^d$  [20]. Furthermore, the small gluon and sea contributions evaluated in the model of Ref. [9] cancel here to a large extent. The asymmetries  $A_{UT}^{\sin \phi_s}$  and  $A_{LT}^{\cos \phi_s}$  represent imaginary and real part, respectively, of the same difference of two products  $\mathcal{M}^* \mathcal{M}$  of two helicity amplitudes, where the first term of this difference represents a combination of GPDs  $H_T$  and  $H$ , and the second a combination of  $\bar{E}_T$  and  $E$ . As can be seen in Fig. 5 and Table 2, while no conclusion can be drawn on  $A_{LT}^{\cos \phi_s}$  because of larger experimental uncertainties, a non-vanishing value for  $A_{UT}^{\sin \phi_s}$  is measured. The asymmetry  $A_{UT}^{\sin(2\phi - \phi_s)}$  represents the same combination of GPDs  $\bar{E}_T$  and  $E$  as the second term in  $A_{UT}^{\sin \phi_s}$ . The observation of a vanishing value for  $A_{UT}^{\sin(2\phi - \phi_s)}$  implies that the non-vanishing value of  $A_{UT}^{\sin \phi_s}$  constitutes the first experimental evidence from hard exclusive  $\rho^0$  leptonproduction for the existence of transverse GPDs  $H_T$ .

## 6. Summary

Asymmetries related to transverse target polarisation were measured in azimuthal modulations of the cross section at COMPASS in exclusive  $\rho^0$  muonproduction on protons. The amplitudes of five single-spin asymmetries for unpolarised beam and three double-spin asymmetries for longitudinally polarised beam were extracted as a function of  $Q^2$ ,  $x_{Bj}$ , or  $p_T^2$ . The asymmetry  $A_{UT}^{\sin \phi_s}$  was found to be  $-0.019 \pm 0.008(\text{stat.}) \pm 0.003(\text{sys.})$ . All other asymmetries were also found to be of small magnitude but consistent with zero within experimental uncertainties. Very recent model calculations agree well with the present results. The results represent first experimental evidence from hard exclusive  $\rho^0$  leptonproduction for the existence of non-vanishing transverse GPDs  $H_T$ .

## Acknowledgements

We gratefully acknowledge the support of the CERN management and staff and the skill and effort of the technicians of our collaborating institutes. This work was made possible by the financial support of our funding agencies. Special thanks go to P. Kroll and S. Goloskokov for providing us with the full set of model calculations as well as for the fruitful collaboration and many discussions on the interpretation of the results.

## References

- [1] S. Meissner, A. Metz, M. Schlegel, *J. High Energy Phys.* 0908 (2009) 056, arXiv:0906.5323;  
S. Meissner, A. Metz, M. Schlegel, K. Goeke, *J. High Energy Phys.* 0808 (2008) 038, arXiv:0805.3165.
- [2] C. Lorcé, B. Pasquini, *J. High Energy Phys.* 1309 (2013) 138, arXiv:1307.4497.
- [3] M. Burkardt, *Phys. Rev. D* 62 (2000) 071503, arXiv:hep-ph/0005108;  
M. Burkardt, *Phys. Rev. D* 66 (2002) 119903 (Erratum).
- [4] M. Burkardt, *Int. J. Mod. Phys. A* 18 (2003) 173, arXiv:hep-ph/0207047.
- [5] A.V. Radyushkin, *Phys. Lett. B* 385 (1996) 333, arXiv:hep-ph/9605431.
- [6] J.C. Collins, L. Frankfurt, M. Strikman, *Phys. Rev. D* 56 (1997) 2982, arXiv:hep-ph/9611433.
- [7] S.V. Goloskokov, P. Kroll, *Eur. Phys. J. C* 42 (2005) 281, arXiv:hep-ph/0501242.
- [8] S.V. Goloskokov, P. Kroll, *Eur. Phys. J. C* 53 (2008) 367, arXiv:0708.3569.
- [9] S.V. Goloskokov, P. Kroll, *Eur. Phys. J. C* 59 (2009) 809, arXiv:0809.4126.
- [10] A.D. Martin, M.G. Ryskin, T. Teubner, *Phys. Rev. D* 55 (1997) 4329, arXiv:hep-ph/9609448.
- [11] X. Ji, *Phys. Rev. Lett.* 78 (1997) 610, arXiv:hep-ph/9603249.
- [12] M. Guidal, M.V. Polyakov, A.V. Radyushkin, M. Vanderhaeghen, *Phys. Rev. D* 72 (2005) 054013, arXiv:hep-ph/0410251.
- [13] K. Kumerički, D. Müller, *Nucl. Phys. B* 841 (2010) 1, arXiv:0904.0458.
- [14] G.R. Goldstein, J.O. Hernandez, S. Liuti, *Phys. Rev. D* 84 (2011) 034007, arXiv:1012.3776.
- [15] M. Guidal, H. Moutarde, M. Vanderhaeghen, *Rep. Prog. Phys.* 76 (2013) 066202, arXiv:1303.6600 [hep-ph].
- [16] M. Diehl, T. Feldmann, R. Jakob, P. Kroll, *Eur. Phys. J. C* 39 (2005) 1, arXiv:hep-ph/0408173.
- [17] A. Airapetian, et al., HERMES Collaboration, *J. High Energy Phys.* 0806 (2008) 066, arXiv:0802.2499.
- [18] M. Mazouz, et al., Jefferson Lab Hall A Collaboration, *Phys. Rev. Lett.* 99 (2007) 242501, arXiv:0709.0450.
- [19] A. Airapetian, et al., HERMES Collaboration, *Phys. Lett. B* 679 (2009) 100, arXiv:0906.5160.
- [20] C. Adolph, et al., COMPASS Collaboration, *Nucl. Phys. B* 865 (2012) 1, arXiv:1207.4301.
- [21] P. Kroll, H. Moutarde, F. Sabatié, *Eur. Phys. J. C* 73 (2013) 2278, arXiv:1210.6975.
- [22] S.V. Goloskokov, P. Kroll, *Eur. Phys. J. C* 65 (2010) 137, arXiv:0906.0460.
- [23] S.V. Goloskokov, P. Kroll, *Eur. Phys. J. A* 47 (2011) 112, arXiv:1106.4897.
- [24] A. Airapetian, et al., HERMES Collaboration, *Phys. Lett. B* 682 (2010) 345, arXiv:0907.2596.
- [25] S.V. Goloskokov, P. Kroll, *Eur. Phys. J. C* 74 (2014) 2725, arXiv:1310.1472;  
S.V. Goloskokov and P. Kroll, private communication.
- [26] M. Diehl, S. Sapeta, *Eur. Phys. J. C* 41 (2005) 515, arXiv:hep-ph/0503023.
- [27] P. Abbon, et al., COMPASS Collaboration, *Nucl. Instrum. Methods A* 577 (2007) 455, arXiv:hep-ex/0703049.
- [28] V.Y. Alekseev, et al., COMPASS Collaboration, *Eur. Phys. J. C* 52 (2007) 255, arXiv:0704.1863.
- [29] M. Arneodo, et al., New Muon Collaboration, *Nucl. Phys. B* 429 (1994) 503.
- [30] B. Adeva, et al., Spin Muon Collaboration, *Phys. Rev. D* 60 (1999) 072004;  
B. Adeva, et al., *Phys. Rev. D* 62 (2000) 079902 (Erratum).
- [31] C. Adolph, et al., COMPASS Collaboration, *Phys. Lett. B* 718 (2013) 922, arXiv:1202.4064.
- [32] A. Tripet, Spin Muon Collaboration, *Nucl. Phys. B (Proc. Suppl.)* 79 (1999) 529, arXiv:hep-ex/9906008.
- [33] A. Airapetian, et al., HERMES Collaboration, *Eur. Phys. J. C* 29 (2003) 171, arXiv:hep-ex/0302012.
- [34] The Durham HepData Project, <http://hepdata.cedar.ac.uk/reaction>.